Dalton Transactions

PAPER

View Article Online
View Journal | View Issue

Cite this: *Dalton Trans.*, 2014, **43**, 6032

A new arene–Ru based supramolecular coordination complex for efficient binding and selective sensing of green fluorescent protein†

Anurag Mishra,‡[a] Sambandam Ravikumar,‡[b,f] Young Ho Song,[a] Nadarajan Saravanan Prabhu,[c] Hyunuk Kim,*[d] Soon Ho Hong,[b] Seyeon Cheon,[e] Jaegeun Noh[e] and Ki-Whan Chi*[a]

Received 11th November 2013,
Accepted 5th December 2013

DOI: 10.1039/c3dt53186d

www.rsc.org/dalton

A new dipyridyl ligand is encoded with 120° angularity between its coordination vectors by using a central pyridine carboxamide scaffold to orient two 4-(pyridin-4-ylethynyl)phenyl moieties. The *N*,*N*′-bis(4-(pyridin-4-ylethynyl)phenyl)pyridine-2,6-dicarboxamide ligand undergoes self-assembly with a diruthenium arene complex to furnish a [2 + 2] metallacycle with a wedge-like structure. The metallacycle binds to the enhanced green fluorescent protein (EGFP) variant of GFP, resulting in steady-state spectral changes in UV-Vis absorption and emission experiments. These studies indicate that the metallacycle induces conformation changes to the EGFP, disrupting the tripeptide chromophore. Furthermore, gel electrophoresis, circular dichroism and atomic force microscopy studies indicate that binding ultimately leads to aggregation of the protein. Computational investigations indicate a favorable interaction, predominantly between the metallacycle and the Arg168 residue of the EGFP. An interaction with Arg168 and related residues was previously observed for an emission-attenuating antibody, supporting that these interactions induce changes to the photophysical properties of EGFP by disrupting the tripeptidechromophore in a similar manner. Additionally, we have also described the quenching study of the reporter GFP protein *in vivo* by a new metal complex using reflected fluorescence microscopy. We anticipate that such metal complexes which can passively diffuse into the cells *in vivo* can serve as potential tools in molecular and drug targeting based biological studies.

Introduction

Over the last decade, there has been growing interest in the interface of inorganic chemistry and biology with an emphasis on the non-covalent interactions of coordination complexes with proteins.[1] Studies of the interactions of metal complexes with proteins are facilitated by the large body of research concerning intercellular regulatory factors and their effects on protein conformations and subsequent functions. Since coordination complexes may behave in a similar fashion to these regulatory factors, non-covalent complex–protein interactions can be investigated by applying analogous techniques in order to probe the mechanism of action of a complex which can involve a variety of pathways including amino acid and side-chain degradation, redox chemistry of thiol and disulfide moieties, aggregation, and tertiary structure changes which can attenuate or halt biological activity.[2]

Supramolecular coordination complexes (SCCs) are congruous with such applications as they exemplify the synthetic ease and tunability associated with metal–ligand bonding.[3] Formed by coordination-driven self-assembly, such constructs can be rapidly generated, affording a number of different 2D and 3D geometries with nuclearities ranging from two metals for small rhomboids, to up to twenty-four or more metals for larger polyhedra.[4]

Ruthenium-based molecules are of particular interest in both supramolecular coordination chemistry[5,6] as well as metal complex–protein interactions due to the metal's controllable coordination environment and inherent biological

[a]*Department of Chemistry, University of Ulsan, Ulsan 680-749, Republic of Korea. E-mail: kwchi@ulsan.ac.kr*
[b]*Department of Chemical and Bioengineering, University of Ulsan, Ulsan 680-749, Republic of Korea*
[c]*School of Biotechnology, Yeungnam University, Gyeongsan 712-749, Republic of Korea*
[d]*Energy Materials and Convergence Research Department, Korea Institute of Energy Research, Daejeon 305-343, Republic of Korea. E-mail: hyunuk@kier.re.kr*
[e]*Department of Chemistry, Hanyang University, 17 Haengdang-dong, Seongdong-gu, Seoul 133 791, Republic of Korea*
[f]*Department of Pharmaceutical Science and Technology, Catholic University of Daegu, Hayang-eup, Gyeongsan-Si, Gyeongbuk 712-702, Republic of Korea*
†Electronic supplementary information (ESI) available: Spectroscopic figures, gel electrophoresis, molecular modeling studies. CCDC 899538. For ESI and crystallographic data in CIF or other electronic format see DOI: 10.1039/c3dt53186d
‡These authors contributed equally.

activity.[7] Meggers and coworkers[8] have demonstrated that octahedral Ru(II) complexes containing bidentate pyridocarbazole ligands are noteworthy in the design of novel transition metal-based drugs wherein they act as inhibitors of protein kinases. Since such inhibition is an attractive vector for developing new anticancer agents, these species are highly relevant in drug development. SCCs utilizing Ru are well-established and typically employ dinuclear arene–Ru(II) building blocks in which the two metal centers are bridged by an oxalate-type ligand. Both 2D and 3D Ru-based SCCs have been investigated in biological settings; however, the majority of this work has focused on interactions with DNA and cell viability studies to investigate potential anticancer activities rather than interactions with other intercellular targets, such as proteins.[9]

Herein, we report the design of a new ditopic ligand as a building block for SCC formation as demonstrated by a [2 + 2] self-assembly of an arene–Ru based complex. The ligand is well-suited to interact with amino acid residues, specifically through its central pyridyl-2,6-dicarboxamide moiety. The amide functionalities offer sites for hydrogen bonding without participating in or disrupting the self-assembly process to furnish an SCC, as evidenced by early examples of complex formation with amide-based dipyridyl donors.[10] Here, the ligand has been spatially tuned *via* the inclusion of ethynyl groups which offer structural rigidity while expanding the conjugated π system to enhance photophysical properties.

Green fluorescent protein (GFP) is a widely used biological marker for gene expression and *in situ* protein interaction studies.[11] Its photophysical properties are sensitive to conformational changes thus providing a spectral handle which can be observed even by the naked eye due to visible emission wavelengths. The enhanced GFP variant (EGFP) was selected for these complex interaction studies due to its ~35 fold increase in emission intensity over wild-type GFP. EGFP is a barrel-shaped protein which possesses a *p*-hydroxybenzylidene–imidazolidone moiety as a chromophore.[12] Post-translational cyclization and oxidation of this sequence produces the chromophore, making its formation highly dependent on proper folding and tertiary structure, and rendering it highly sensitive to agents which can induce conformational changes.[13]

As a pioneering example of the interaction of Ru macrocycles with GFP, we believe that this work provides an important foundation in the design of new protein–SCC systems which will motivate broader targets, including new therapeutics, novel biosensors, and strategies for the separation of peptide mixtures using metal complexes.

Results and discussion

Synthesis and characterization of ligand 1

The new ligand **1** was synthesized in two steps. The first starting ligand precursor *N*,*N*′-bis(4-iodophenyl)pyridine-2,6-dicarboxyl-amide was synthesized by coupling of pyridine-2,6-dicarbonyl chloride and 4-iodoaniline in CH_2Cl_2 in the presence of triethylamine (Scheme 1).

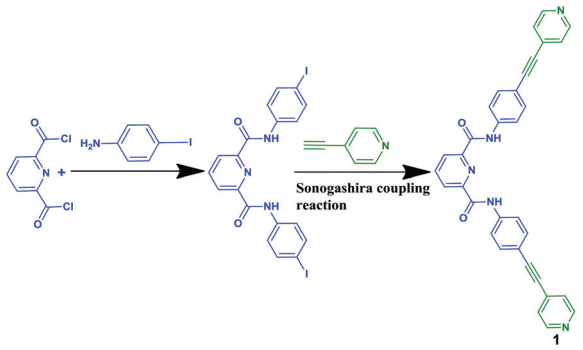

Scheme 1 Synthesis of ligand **1**.

The resulting product was then used under standard Sonogashira coupling conditions with the hydrochloride salt of 4-ethynylpyridine in DMF to generate **1** in *ca.* 50% overall yield. In the IR spectrum of the product, NH and CO stretching peaks for the amide linkage were observed at 3366 and 1690 cm^{-1} respectively, while C≡C was at 2216 cm^{-1}. The ^1H NMR showed one broad singlet for the NH at δ 10.18 in nitromethane-d_3, and the six aromatic resonances were found to integrate to twelve protons (Fig. S1†).

Synthesis and characterization of metallacycle 1

The [2 + 2] self-assembly of ligand **1** with Ru-acceptor **2** was carried out in methanol solution in the presence of AgOTf (OTf = triflate) which furnished a wedge-shaped tetracationic complex **3** as a triflate salt along with AgCl. For use in control experiments, **2** was also combined with 4,4′-bipyridine and 1,3-bis(3-pyridylethynyl)benzene to generate related [2 + 2] metallacycles **4** and **5** respectively (see Scheme 2) which lacked the hydrogen bonding.[14,15]

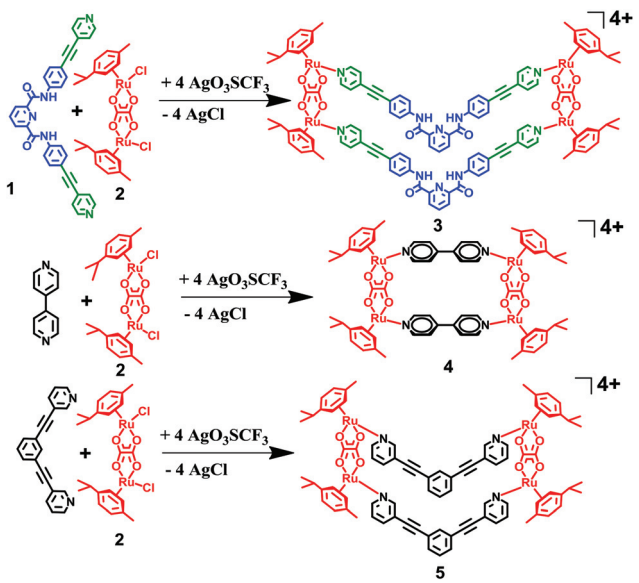

Scheme 2 Synthesis of metallacycles **3–5**.

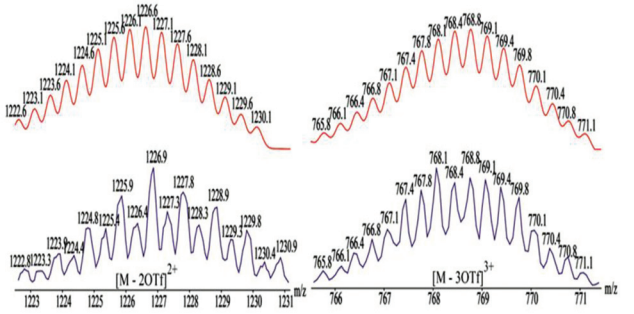

Fig. 1 Theoretical (red, top) and experimental (blue, bottom) ESI-MS regions corresponding to $[3 - 2OTf]^{2+}$ (left) and $[3 - 3OTf]^{3+}$ (right) charge states of **3**.

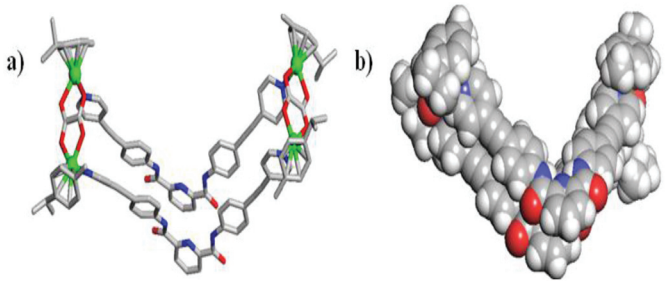

Fig. 2 (a) The structure of **3** reveals a [2 + 2] assembly. (b) Space filling model of **3**.

The structural assignment of **3** as a [2 + 2] complex was initially indicated by its ^{1}H NMR spectrum in nitromethane-d_3, which revealed chemical shift changes relative to those observed for **1**, the most significant being the large upfield shifts of the H_α terminal pyridyl protons (Fig. S3†). The idealized C_{2v} symmetry of **3** results in a highly symmetric core that manifests in a relatively simple aromatic region in the ^{1}H and ^{13}C NMR spectra (Fig. S3 and S4†).

Electron-spray ionization mass spectrometry (ESI-MS) was employed to further confirm the [2 + 2] nature of **3**. The spectrum of **3** showed peaks at m/z = 1126.9 and 768.8 which correspond to $[M - 2OTf]^{2+}$ and $[M - 3OTf]^{3+}$, respectively, and consistent with their theoretical isotopic distributions (Fig. 1).

The electronic absorption spectrum of **3** along with its precursors reveals that the transitions associated with the free ligand **1** are largely preserved upon self-assembly (Fig. S5a†). The dominant spectral features of complex **3** match closely with those of ligand **1**, albeit with minor bathochromic shifts. As such, the large band centered at 328 nm is assigned to a ligand-based $\pi\rightarrow\pi^*$ transition, with the slight red shift (~8 nm) relative to the free ligand likely due to contributions from metal-to-ligand charge transfers which are introduced upon Ru coordination. Similar bands are maintained between **3** and **1** at higher energies, which support that these features are also ligand-centered. While **2** shows minor bands past its shoulder at ~200 nm, the low signal of these bands causes them to be lost amidst the ligand centered transitions found in **3**. Despite the normalized concentrations, the absorbance of **3** is not significantly higher than **1**, despite containing two ligands per molecule. This suggests that the individual ligands are not electronically isolated in **3**, which is not unsurprising given that all the organic fragments present in **3** possess π systems to facilitate coupling.

The strongest evidence for the structural assignment of **3** is given by a single crystal X-ray diffraction analysis. Crystals suitable for structural analysis were grown by the slow diffusion of diethyl ether into solutions of **3** in nitromethane. The resulting structure, shown in Fig. 2, reveals that the [2 + 2] assembly of **1** and **2** produces a wedge-shaped complex with approximately C_{2v} symmetry (Fig. S18†). The two ligands bridge in a cofacial arrangement rather than remaining in-plane as seen for 2D rhomboid and rectangular assemblies. This conformation reduces the strain on the Ru coordination sphere associated with rhomboid formation using a 120° ligand. The distance between Ru(II) centers is 5.4 × 21.5 Å^2, which is the dimension of the wedged pocket. Each Ru center reflects the coordination sphere expected from precursor **2**, specifically consisting of a η^6-*p*-cymene ligand, two oxygen atoms from the bridging oxalate ligand and coordination from a terminal pyridyl group of ligand **1**. The average Ru–N and Ru–O distances are 2.08 and 2.12 Å, respectively, which are comparable to those found in other oxalato-bridged [2 + 2] assemblies.[10b] The N–Ru–O bite angles range from 78.1(2)° to 87.8(2)°, indicating a noticeable distortion from the idealized 90° angles expected in a *cis*-capped octahedral coordination sphere. The internal pocket of **3** was not occupied by solvent molecules or triflate counterions.

Green fluorescent protein binding study

The binding affinity of **3** for EGFP was initially investigated using electronic absorption spectroscopy. The UV-vis absorption spectrum of EGFP contains high energy bands at ~280 nm which have been assigned to tryptophan (Trp) and tyrosine (Tyr) residues.[16] The central Thr65-Tyr66-Gly67 tripeptide sequence of the protein represents a chromophore and provides a relatively low energy absorption band at 488 nm.[17] Upon the addition of EGFP to a solution of **3** (Fig. 3a), the 350 nm band of the complex decreased commensurate with an

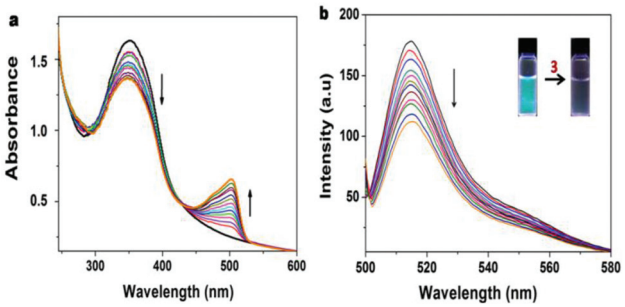

Fig. 3 (a) UV-vis absorption spectra of **3** (20 μM) upon incremental addition of EGFP (0–26 μM). (b) Emission spectra of EGFP (2×10^{-6} M) upon gradual addition of **3** (0–20 μM).

absorption growth at 500 nm, corresponding to the low-energy band of the protein. The significant hypochromic shift at 350 nm and hyperchromic shift at 500 nm are evidence of an interaction between EGFP and complex **3**, as the band at 350 nm would not otherwise decrease.

We next investigated the binding of the complexes to EGFP by a fluorescence spectroscopic method. The emission behavior of EGFP was significantly affected by the addition of **3**; however in the case of **4** and **5** (Scheme 2), no major significant changes were observed (Fig. S8 and S9†). Fig. 3b shows the attenuation of the emission band at 512 nm with an excitation wavelength of 488 nm in a Tris-HCl buffer medium. The steady decrease in signal intensity upon the addition of **3** indicates a disruption in either the tertiary or secondary structure of EGFP which renders the tri-peptide chromophore sequence unable to form the necessary *p*-hydroxybenzylidene–imidazolidinone moiety which is responsible for emission.

The Stern–Volmer constants (K_{SV}) calculated for **3** were 7.5×10^8 M^{-1} (r = 0.98) (Fig. S10†). The large binding constants, which agree well with the Stern–Volmer constants, are evidence of strong EGFP binding with **3**.

The spectral changes at 512 nm were used to quantify the binding constant of this interaction. The magnitude of the binding constants (K) was calculated to be 7.394×10^8 M^{-1} (Fig. S11†).

Since the photophysical studies of **3** with EGFP indicated that strong interactions were occurring between the complex and the protein, time-dependent protein cleavage assays were employed to further probe the nature of the binding. As shown in Fig. 4, the gels exposed to both UV light and Coomassie blue stain indicate that no cleavage of EGFP was induced by **3** due to the lack of any bands at a lower molecular weight than the protein; however, bands were present at higher molecular weights, specifically at 50 and 81 kDa. Analogous assays were also carried out with precursors **1** and **2**, which did not exhibit any cleavage, fading or smearing, nor were bands observed at higher molecular weight to suggest aggregation (see Fig. S12†).

To further probe whether complex **3** acts as a selective sensor for EGFP and to determine the nature of this aggregation, we carried out experiment involving interaction of **3** with other proteins (BSA & ovalbumin). Fig. S13† exhibits no significant change in the bands suggesting **3** as a selective sensor. To further probe the nature of this aggregation, the assay was run once more using metallacycles **4** and **5** (Scheme 2). Both control compounds lacked amide protons and carbonyl oxygen atoms and were expected to thus lack the ability to hydrogen bond and bind strongly to EGFP. The SDS–PAGE result from this assay suggested that there was a cleavage in the EGFP bands but no aggregation was observed (Fig. S14 and S15†). As such, the amide functionalities of **3** appear necessary for protein interaction and subsequent aggregation to occur.

Next, we studied the ability of **3** to induce the conformational changes in EGFP by circular dichroism. This result also strongly supports that **3** destabilizes the EGFP conformation, but no major changes were observed on BSA. To study the specificity of denaturing ability of **3**, the same assay was also carried out with **4** and **5** which makes no significant changes in the conformation of EGFP and BSA (Fig. 5 and S16†).

The ability of **3** to induce aggregation of EGFP was further investigated using atomic force microscopy (AFM). The images clearly show a significant change in the surface morphology of EGFP after treatment with **3** (Fig. 6). In the absence of **3**, the EGFP produces a relatively uniform coverage of the mica surface with molecular spots possessing lateral dimensions of 10–30 nm. Upon treatment with **3**, this uniformity was removed and the material aggregated to produce globular structures with lateral dimensions of 40–100 nm. This result strongly supports that **3** induces aggregation of EGFP which is consistent with the binding interactions revealed by prior experiments. A control sample of EGFP treated with **4** does not exhibit aggregation and the mica surface remains uniform,

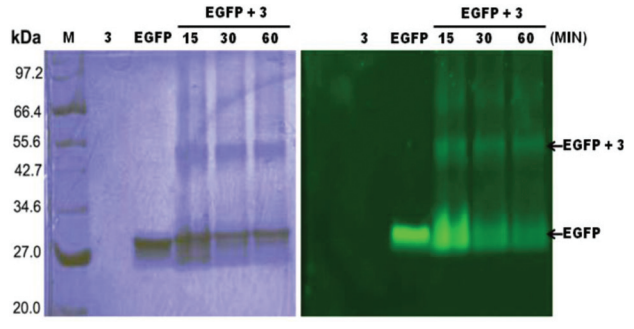

Fig. 4 SDS–PAGE of EGFP (5 μM) incubated at 37 °C with **3** (10 μM) in a 5% DMSO/10 mM Tris-HCl buffer (pH = 7.0) exposed to Coomassie blue stain (left) and UV light (right).

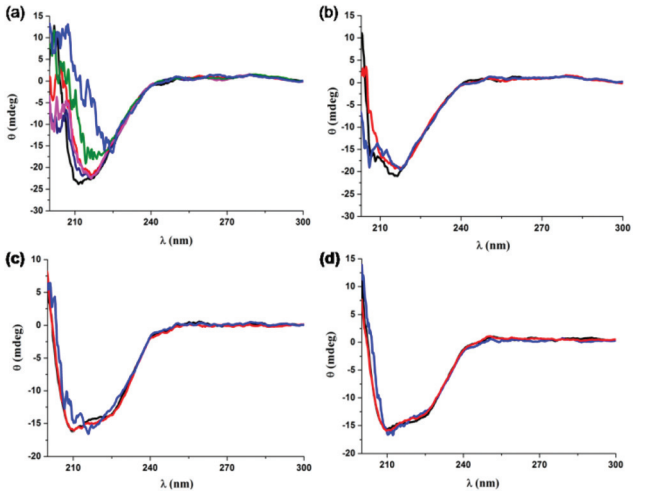

Fig. 5 Circular dichroism of different proteins in the presence of **3** and **4** (10 mM Tris-HCl buffer, pH 7.0). (a) CD spectrum of 11.2 μM EGFP upon titration with **3** (0, 1.6, 3.3, 5.0, 6.6 and 8.3 μM). (b) CD spectra of EGFP (11.2 μM) in the absence and presence of **4** (5.0 and 8.3 μM). (c) CD spectra of BSA (8.5 μM) in the absence and presence of **3** (5.0 and 8.3 μM). (d) CD spectra of BSA (8.5 μM) in the absence and presence of **4** (5.0 and 8.3 μM).

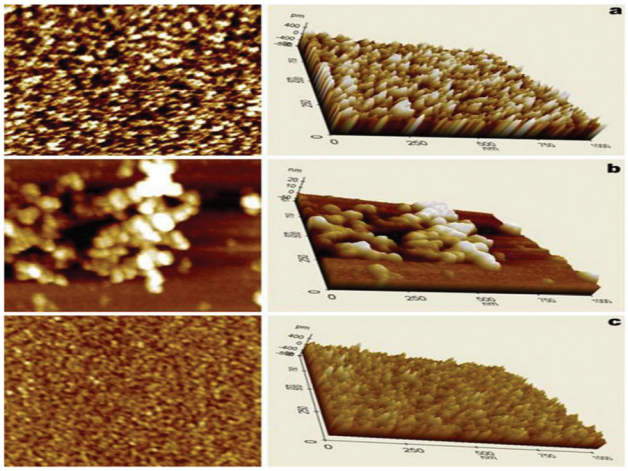

Fig. 6 Circular AFM images (1 μm × 1 μm) of the mica surfaces: (a) EGFP alone, (b) EGFP after treatment with **3** and (c) EGFP after treatment with **4**. A drop of 7.5 ng μL^{-1} aqueous solutions on mica surfaces were incubated for 5 min and dried under N_2 gas stream.

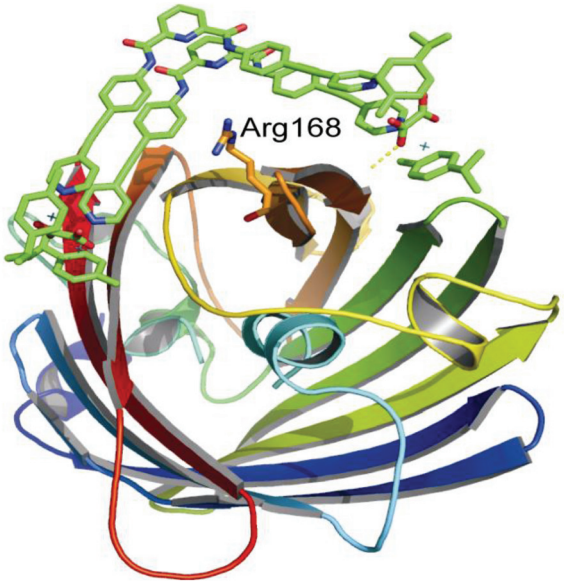

Fig. 7 Close view of the interaction between **3** and EGFP.

further confirming that the unique moieties present in **3** are critical for these interactions.

Furthermore, the interactions between **3** and EGFP were predicted using molecular modeling studies. As the crystal structure of our EGFP variant was not available, we attempted to develop a 3D model structure for the EGFP based on related, known structures. A template search for our variant using BlastP revealed a GFP structure that differed by only a single amino acid in the chromophore (Table 1 in ESI†). In addition, we also analyzed two templates of EGFP co-crystallized with two specific nanobodies. A recent report by Kirchhofer describes two camelid-derived single-domain antibodies (nanobodies), one of which induced a 5-fold decrease in emission intensity, the other effecting a 10-fold increase.[18] The attenuating antibody, dubbed *the minimizer* in contrast to its *enhancer* counterpart, was found to interact with the Arg168 residue of the protein which is proximal to the chromophore tri-peptide sequence.

This interaction shifted the His148 residue away from the chromophore, causing Arg168 to lose its interaction with Asn146, the ultimate effect being an overall conformational change sufficient to affect emission. One established strategy for predicting the interactions between a novel inhibitor and a protein is to make comparisons with the mechanism of a known inhibitor of that same protein.[19] As such, our GFP variant was modeled using both the minimizer and enhancer nanobody-bound EGFP structures and docking studies were carried out with models of **3**. The computational results indicated that **3** gave better docking models when interacting with the minimizer-derived conformation of EGFP, shown in Fig. 7 and S17.† Since **3** clearly stabilizes a fluorescence-attenuated confirmation of the protein relative to the native structure and emission-enhanced structure, it follows that the complex may act by inducing similar conformational changes, leading to a quenching effect.

In vivo study

Synthetic molecules can serve as a potential tool in the molecular and drug targeting based biological studies. One of the innumerable applications offered by such synthetically designed complexes is that they can passively diffuse into the cells and deactivate the target bio-molecules at the cellular level. To investigate the interference of complex **3** with the fluorescent reporter protein *in vivo*, reflected fluorescence microscopy was carried out. Fluorescence induced *E. coli* cells harboring pET21a-GFP were incubated with 1 mM of complex **3** at different time intervals. In relation to *in vitro* studies, quenching of the EGFP was also observed *in vivo* from 1 to 6 h incubation of **3** (Fig. 8). The

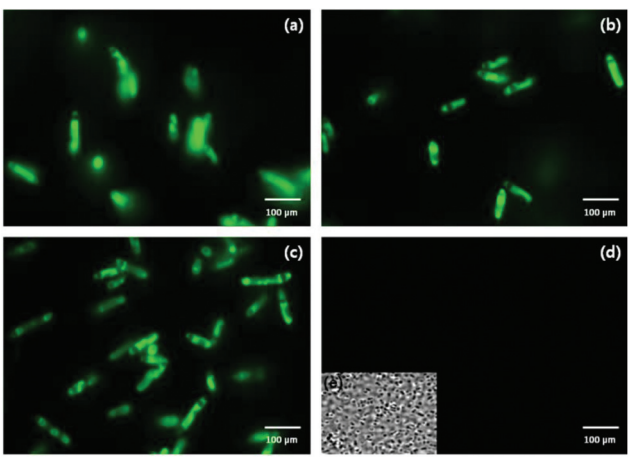

Fig. 8 Reflected fluorescence microscopy images of an *E. coli* BL21 carrying pET21a-EGFP incubated in the presence and absence (a) of complex **3** (1 mM) after induction with 1 mM of IPTG for the identification of cellular uptake for complex **3** into these bacterial strains after 1 h (b), 2 h (c) and 6 h (d) of incubation. (e) Insets give DIC image of complex **3** incubated for 6 h with bacterial strain.

fluorescence emitted by the GFP protein was found to be completely quenched after 6 h in the incubation of the bacterial cells with complex **3**. Quenching of the EGFP within the cellular cytosol further indicates the membrane permeable trait of complex **3**. In this respect, complex **3** mediated deactivation of the target biomolecule might become an attractive source for future studies with relevance to drug delivery, targeting and biosensing through complex–protein interactions.

Conclusions

In conclusion, we report here the first studies of protein interactions of Ru-based SCCs using a novel [2 + 2] assembly encoded with moieties capable of non-covalent interactions with amino acid residues. A high-yielding self-assembly furnished **3**, as confirmed by NMR, ESI-MS and X-ray crystallography. The roughly C_{2v} symmetric, wedge-shaped SCC **3** was found to strongly bind to EGFP, altering the photophysical properties of the protein, as probed by steady-state UV-vis and emission binding experiments. This binding was further probed by gel electrophoresis, circular dichroism and AFM studies which indicate that EGFP undergoes aggregation in the presence of **3**, but not its precursors, nor a related SCC which lacked hydrogen bonding functionalities. Molecular modeling validated the proposed quenching mechanism by revealing that **3** likely acts in a similar manner to a known emission-attenuating antibody, disrupting the chromophore of EGFP *via* conformational changes. Additionally, we also described the quenching study of the reporter GFP protein *in vivo* by a new metal complex, using reflected fluorescence microscopy. Studies to further elaborate the mechanism for protein binding and potential selectivity of the complex with other GFP variants are underway.

Materials and methods

All chemicals used in this work were purchased from commercial sources and used without further purification. All solvents used were distilled by standard methods. Precursors **2** and **4** were prepared according to the literature.[14] The ^{1}H and ^{13}C NMR spectra were recorded on a Bruker 300 MHz spectrometer. The chemical shifts (δ) in the ^{1}H NMR spectra were reported relative to tetramethylsilane (Me_4Si) as an internal standard (0.0 ppm). Mass spectra were recorded on a Micromass Quattro II triple-quadrupole mass spectrometer using electrospray ionization (ESI) and processed using the MassLynx software suite. Elemental analyses were performed using a Perkin-Elmer CHN analyzer. Absorption spectra were recorded using a Cary 100 Conc UV-Visible spectrophotometer. Fluorescence titration studies were carried out on a RF-5301PC spectrofluorimeter (Shimadzu, Japan). PCR reagents, T4 DNA ligase and restriction endonucleases were purchased from Promega (Madison, WI, USA). The isopropyl-D-thiogalactopyranoside (IPTG) was purchased from Sigma (St. Louis, MO, USA). The host bacterium *Escherichia coli* (*E. coli*) strain XL1-blue (Stratagene, CA, USA) was used for plasmid DNA preparation in this study. The nickel nitrilotriacetic acid (Ni-NTA) affinity column was purchased from Qiagen (Valencia, CA, USA). The e*gfp* gene was amplified from the plasmid pROBE-NT′ and subsequently cloned into pET21a using restriction enzyme. The construct pET21a-EGFP was transformed into *E. coli* BL21.

X-ray crystallography for 3

The diffraction data from a single crystal of **3** mounted on a loop were collected at 100 K on an ADSC Quantum 210 CCD diffractometer with synchrotron radiation (λ = 0.80000 Å) at the Macromolecular Crystallography Beamline 6B1, Pohang Accelerator Laboratory (PAL), Pohang, Korea. The raw data were processed and scaled using the program HKL2000. The structure was solved by direct methods, and the refinements were carried out with full-matrix least-squares on F^2 with appropriate software implemented in SHELXTL software suite. All the non-hydrogen atoms were refined anisotropically. Hydrogen atoms were added to their geometrically ideal positions except solvent molecules (acetone and methanol). The crystallographic data are summarized in Table S2.† CCDC 899538 contains the supplementary crystallographic data for this paper.

UV-Vis binding study

Absorption spectra were recorded using a Cary 100 Conc UV-Visible spectrophotometer. The spectral changes were observed upon the addition of 0–26 μM EGFP to a 20 μM solution of **3** and addition of a 0–32 μM solution of **3** to a 20 μM EGFP in 10 mM of Tris-HCl solution.

Fluorescence binding study

Fluorescence spectra of control and test proteins were recorded on a RF-5301PC spectrofluorimeter (Shimadzu, Japan). The emission behavior of EGFP was significantly affected by the addition of **3**. An excitation wavelength of 488 nm shows the attenuation of the emission band at 512 nm with in a Tris-HCl buffer medium. The steady decrease in signal intensity upon the addition of **3** indicates a disruption in either the tertiary or secondary structure of EGFP which renders the tri-peptide chromophore sequence unable to form the necessary *p*-hydroxybenzylidene–imidazolidinone moiety which is responsible for emission. The spectral changes which occur when **3** is present in a solution of EGFP suggest that the complex could be used as a sensor for this and related proteins. Generally, a linear Stern–Volmer (SV) plot was used to a 1 : 1 binding model for fluorescence quenching to get a linear relationship. In order to gain insight into the quenching mechanism, the fluorescence quenching data for complex **3** were analysed by using the Stern–Volmer equation.

$$\frac{I_0}{I} = 1 + K_{sv}[\mathbf{3}] \quad (1)$$

where I_0 and I are the fluorescence intensities of EGFP in the absence and in the presence of the quencher, [**3**] is the concentration of the quencher and K_{sv} is the Stern–Volmer constant. The displayed Stern–Volmer plots showed that within the investigated concentrations, the results agreed with the Stern–Volmer equation.

The fluorescence quenching data obtained from the interaction of complex **3** with EGFP were further analyzed in order to obtain binding parameters by using the equation

$$\log\left[\frac{I_0 - I}{I}\right] = \log K + n\log[\mathbf{3}] \quad (2)$$

where I_0 and I are the fluorescence intensity in the absence and in the presence of complex **3**. Plots of $\log[(I_0 - I)/I]$ *versus* log [**3**] gave a straight line whose slope provided n, the number of binding sites, while the intercept allowed the calculation of the values of apparent binding constant, K, specifying the number of **3** bound to a EGFP macromolecule, whose slope was equal to n and the intercept on the y axis to log K. The value of n is approximately equal to 1 which indicated the existence of just a single binding site in EGFP for **3**. The value of binding constant K, 7.394×10^8 M^{-1}, showed strong interaction between EGFP and **3**.[20]

Protein purification

The above mentioned construct was cultivated in a Luria–Bertani medium supplemented with ampicillin at 37 °C with vigorous shaking. When the optical density of the culture reached 0.8 to 1.0 at 600 nm, 1 mM of IPTG was added to induce protein expression. OD600 was then measured and the cells were harvested after 6 h of induction. Harvested cells were stored at −70 °C until used. Cell lysis was carried out using a Bug Buster protein extraction kit (Novagen) followed by sonication. Cell pellets corresponding to 1 mL of culture were resuspended in 100 μl of lysis buffer, incubated at room temperature for 10 min, and centrifuged at 9000*g* at 4 °C for 20 min. The supernatant was saved as a soluble protein fraction, and analyzed by SDS–PAGE (10% acrylamide gel). The recombinant proteins were purified from the soluble protein fraction by using an Ni-NTA affinity column. His-tag purified samples were subjected to gel permeation chromatography (GPC) by an AKTA Explorer FPLC system containing a Superdex 75 HR column at 4 °C. The concentration of the protein was quantified using the Bradford assay.

Time dependent protein binding assays using SDS–PAGE

A 5 μM solution of EGFP in Tris-HCl buffer medium (pH 7.0) was incubated at 37 °C with 10 μM of **3** at time intervals ranging from 15 to 60 min. Aliquots of the reaction mixtures were subjected to modified 10% SDS–PAGE (without thermal denaturation). The gel was subsequently rinsed with distilled water and exposed to a UV transilluminator to detect fluorescence bands. The gels were then stained with Coomassie blue stain.

Molecular modeling studies

Homology modeling. The protein sequence of the EGFP variant was translated from the nucleotide sequence using the online tool SMS2. A template search for the EGFP variant sequence was carried out using BlastP against the PDB database.[21] From the Blast result, the EGFP protein structures which had co-crystallized with antibodies were chosen based on how well they matched the EGFP variant used here. Models using both the minimizer and enhancer-bound EGFP were developed and validated using the SAVES server.

Molecular docking. The validated model structures were docked with **3** using GOLD4.1.2. Prior to docking calculations, all hydrogen atoms and charges were added to the protein using Discovery studio2.1. The grid size was set to 10, centered on the *XYZ* co-ordinate of Arg168. The Lamarckian genetic algorithm was employed as a search parameter. Fifty genetic algorithms were run for the docked models. From the fifty solutions thus obtained for each model, the best solution was selected and exported in PDB format and analyzed using Pymol.[22]

Circular dichroism. CD measurements were performed on a JASCO J-715 instrument using quartz 0.1 cm cuvettes. The machine settings were as follows: J-715 scan settings; 600 nm–190 nm scan range, 0.2 nm pitch, continuous scanning at 100 nm min^{-1}, 100 mdeg sensitivity, 4 s response time, 1.0 nm band width, single scan accumulation.

Preparation of *N*,*N*′-bis(4-iodophenyl)pyridine-2,6-dicarboxamide. A solution of 2,6-pyridinedicarbonyl dichloride (1.0 g, 4.90 mmol) and triethylamine (3 mL) in 30 mL of CH_2Cl_2 was prepared and chilled to 4 °C in an ice-bath for 5 min, after which 4-iodo aniline (2.25 g, 10.30) was added slowly over a period of 10 min. The reaction mixture was stirred at room temperature overnight. The resulting precipitate was collected on a frit, recrystallized with MeOH–H_2O, and dried in a vacuum oven. Yield, *ca.* 90% (2.50 g). M.P. = 273 °C, MS (*m*/*z*): calcd = 569.13, found = 569.16. Anal. Calcd for $C_{19}H_{13}I_2N_3O_2$: C, 40.10%; H, 2.30%; N, 7.38%; Found: C, 40.08%; H, 2.22%; N, 7.50%; ^{1}H NMR (d_6-DMSO, 300 MHz, δ, ppm): 11.07 (*s*, 2H, CONH), 8.40 (*d*, 2H, J = 7.5 Hz, H_b), 8.30 (t, 1H, H_a), 7.79–78 (m, 8H; H_d/H_c).

Synthesis of *N*,*N*′-bis(4-(pyridin-4-ylethynyl)phenyl)pyridine-2,6-dicarboxamide 1. In a flame-dried Schlenk flask, 4-ethynylpyridine hydrochloride (0.590 g, 4.2 mmol) and triethylamine (6 mL) were vigorously stirred for 20 min. During this time a white precipitate formed. DMF (30 mL), $Pd(PPh_3)_2Cl_2$ (0.050 g, 0.07 mmol), PPh_3(0.018 g, 0.07), CuI (0.014 g, 0.07 mmol), and *N*,*N*′-bis(4-iodophenyl)pyridine-2,6-dicarboxamide (0.800 g, 1.40 mmol) were successively added. The Schlenk flask was wrapped in aluminum foil to keep the reaction mixture in the dark and the solution was refluxed for 24 h. The resulting brown mixture was filtered on frit, and recrystallized with CH_3OH–H_2O (1 : 1). The compound was filtered and dried under vacuum. Yield, *ca.* 55% (0.400 g). M.P. = 297 °C, MS (*m*/*z*): calcd = 519.55, found = 519.56. Anal. Calcd for $C_{33}H_{21}N_5O_2$: C, 76.29; H, 4.07; N, 13.48; found: C, 76.32; H, 4.11; N, 13.49. IR (KBr, ν, selected peaks): 3366 (NH), 2216

(C≡C), and 1690 (C═O) cm^{-1}; λ_{max}/nm = CH_3OH (ε, dm^3 mol^{-1} cm^{-1}): 320 (1500). ^1H NMR (nitromethane-d_3, 300 MHz, δ, ppm): 10.18 (*s*, 2H, CONH), 8.61 (*d*, 4H, *J* = 6 Hz, H_a), 8.52 (*d*, 2H, *J* = 8.1 Hz, H_e), 8.34–8.29 (*t*, 1H, H_f), 8.02 (*d*, 4H, *J* = 6 Hz, H_b), 7.70 (*d*, 4H, *J* = 6.6 Hz, H_d), 7.48 (*d*, 4H, *J* = 5.7 Hz, H_c); ^{13}C NMR (DMSO-d_6, 300 MHz, δ, ppm): 161.87(C═O, C_{10}), 149.99(C_{11}), 148.59(C_{13}), 140.23(C_{13}), 139.30(C_9), 132.60(C_7), 130.35(C_3), 125.73(C_2), 125.31(C_{12}), 120.78(C_8), 116.61(C_6), 93.79(C_5), 86.51(C_4).

Synthesis of metallacycle 3

A mixture of **2** (50 mg, 0.08 mmol) and 2 equiv. of $AgCF_3SO_3$ (42 mg, 0.16 mmol) in methanol was stirred at room temperature for 2 h and filtered to remove AgCl. Ligand **1** (42 mg, 0.08 mmol) was added to the filtrate. The mixture was then stirred at room temperature for 12 h, and the solvent was removed under reduced pressure. The crude product thus obtained was redissolved in nitromethane and subjected to vapour diffusion of diethyl ether. This resulted in the crystallization of the product over the course of a week. The product was filtered and dried under vacuum. Yield: 100 mg (91%). Anal. Calcd for $C_{114}H_{98}F_{12}N_{10}O_{24}Ru_4S_4$: C, 49.74; H, 3.59; N, 5.09; S, 4.66; found: C, 49.80; H, 3.72; N, 5.12; S, 4.35. FT-IR spectrum (KBR, ν, selected peaks): 3340(NH), 2245 (C≡C), 1620 (C═O) cm^{-1}. MS (ESI) calcd for $[M - 2OTf]^{2+}$ *m*/*z* 1226.6, found 1226.9; calcd for $[M - 3OTf]^{3+}$ *m*/*z* 768.8, found 768.8. Absorption spectrum [λ_{max}/nm, CH_3OH (ε, M^{-1} cm^{-1}): 328 (1600). ^1H NMR (nitromethane-d_3, 300 MHz, δ, ppm): 9.79 (*s*, 4H, CONH), 8.14 (*d*, 8H, *J* = 9.0, H_a), 8.01 (*d*, 8H, *J* = 6.6, H_e), 7.95 (*t*, 4H, H_f), 7.72 (*d*, 8H, *J* = 8.7, H_d), 7.42–7.37 (*m*, 16H, H_c/H_b), 5.89 (*d*, 8H, *J* = 8.7, $-C_6H_4$), 5.72 (*d*, 8H, *J* = 8.7, $-C_6H_4$), 2.90 (*m*, 4H, $-CH(CH_3)_2$), 2.07 (*s*, 12H, $-CH_3$), 1.39 (*d*, 12H, $-CH(CH_3)_2$). ^{13}C NMR (DMSO-d_6, 300 MHz, δ, ppm): 162.22 (C═O), 153.37, 149.53, 141.10, 140.76, 136.86, 134.68, 128.71, 120.69, 117.71, 104.23, 101.46, 86.51, 83.38, 82.97(C═C), 32.48, 22.45, 18.31, 15.66.

Acknowledgements

This work was supported by the Basic Science Research program through the National Research Foundation of Korea (NRF) funded by the Ministry of Science, ICT and Future Planning (NRF-2013R1A1A2006859). The Priority Research Centers program (2009-0093818) through the NRF is also appreciated for financial support. X-ray diffraction experiments using synchrotron radiation were performed at the Pohang Accelerator Laboratory in Korea. We thank Prof. Seok-Kyu Kim and Dr Yoon Jung Jang, Department of Chemistry, Yeungnam University, for providing the circular dichroism facility.

Notes and references

1 (*a*) A. Vergara, I. R. Krauss, D. Montesarchio, L. Paduano and A. Merlino, *Inorg. Chem.*, 2013, **52**, 10714; (*b*) A. Vergara, G. D'Errico, D. Montesarchio, G. Mangiapia, L. Paduano and A. Merlino, *Inorg. Chem.*, 2013, **52**, 4157; (*c*) K. J. Kilpin and P. J. Dyson, *Chem. Sci.*, 2013, **4**, 1410; (*d*) M. Patra and G. Gasser, *ChemBioChem*, 2012, **13**, 1232; (*e*) E. Meggers, *Chem. Commun.*, 2009, 1001; (*f*) N. P. E. Barry and P. J. Sadler, *Chem. Commun.*, 2013, **49**, 5106; (*g*) T. Reiner, D. Jantke, A. N. Marziale, A. Raba and J. Eppinger, *Chem. Open*, 2013, **2**, 50.

2 (*a*) N. P. E. Barry and P. J. Sadler, *Chem. Soc. Rev.*, 2012, **41**, 3264; (*b*) D. J. Clymer, C. R. Geren and K. E. Ebner, *Biochemistry*, 1976, **15**, 1093; (*c*) E. A. Permyakov, S. E. Permyakov, G. Y. Deikus, L. A. Morozova-Roche, V. M. Grishchenko, L. P. Kalinichenko and V. N. Uversky, *Proteins*, 2003, **51**, 498.

3 (*a*) C. K. McLaughlin, G. D. Hamblin and H. F. Sleiman, *Chem. Soc. Rev.*, 2011, **40**, 5647; (*b*) R. Kieltyka, P. Englebienne, J. Fakhoury, C. Autexier, N. Moitessier and H. F. Sleiman, *J. Am. Chem. Soc.*, 2008, **130**, 10040; (*c*) S. Shanmugaraju, A. K. Bar and P. S. Mukherjee, *Organometallics*, 2010, **29**, 2971; (*d*) A. K. Bar, S. Shanmugaraju, K.-W. Chi and P. S. Mukherjee, *Dalton Trans.*, 2011, **40**, 2257; (*e*) S. Shanmugaraju, S. A. Joshi and P. S. Mukherjee, *Inorg. Chem.*, 2011, **50**, 11736.

4 (*a*) R. Chakrabarty, P. S. Mukherjee and P. J. Stang, *Chem. Rev.*, 2011, **111**, 6810; (*b*) Y.-F. Han, W.-G. Jia, W.-B. Yu and G.-X. Jin, *Chem. Soc. Rev.*, 2009, **38**, 3419; (*c*) Y.-F. Han, Y.-J. Lin, W.-G. Jia and G.-X. Jin, *Organometallics*, 2008, **27**, 4088; (*d*) Y.-F. Han, Y.-J. Lin, W.-G. Jia, L.-H. Weng and G.-X. Jin, *Organometallics*, 2007, **26**, 5848; (*e*) Y.-F. Han, Y.-J. Lin, W.-G. Jia, G.-L. Wang and G.-X. Jin, *Chem. Commun.*, 2008, 1807; (*f*) Y.-F. Han, H. Li and G.-X. Jin, *Chem. Commun.*, 2010, **46**, 6879; (*g*) Y.-F. Han, W.-G. Jia, Y.-J. Lin and G.-X. Jin, *Angew. Chem., Int. Ed.*, 2009, **48**, 6234; (*h*) Y.-F. Han, Y. Fei and G.-X. Jin, *Dalton Trans.*, 2010, **39**, 3976.

5 A. Mishra, S. C. Kang and K.-W. Chi, *Eur. J. Inorg. Chem.*, 2013, 5222.

6 (*a*) V. Vajpayee, Y. H. Song, T. R. Cook, H. Kim, Y. Lee, P. J. Stang and K.-W. Chi, *J. Am. Chem. Soc.*, 2011, **133**, 19646; (*b*) K. Severin, *Chem. Commun.*, 2006, 3859; (*c*) B. Therrien, G. Süss-Fink, P. Govindaswamy, A. K. Renfrew and P. J. Dyson, *Angew. Chem., Int. Ed.*, 2008, **47**, 3773; (*d*) A. Mishra, H. Jung, J. W. Park, H. K. Kim, H. Kim, P. J. Stang and K.-W. Chi, *Organometallics*, 2012, **31**, 3519; (*e*) A. Mishra, S. Lee, H. Kim, T. R. Cook, P. J. Stang and K.-W. Chi, *Chem. Asian J.*, 2012, **7**, 2592; (*f*) B. Kilbas, S. Mirtschin, T. R.-Johannessen, R. Scopelliti and K. Severin, *Inorg. Chem.*, 2012, **51**, 5795; (*g*) A. Pitto-Barry, N. P. E. Barry, O. Zava, R. Deschenaux, P. J. Dyson and B. Therrien, *Chem.–Eur. J.*, 2011, **17**, 1966; (*h*) S. Shanmugaraju, A. K. Bar and P. S. Mukherjee, *Inorg. Chem.*, 2010, **49**, 10235; (*i*) B. Kilbas, S. Mirtschin, T. Riis-Johannessen, R. Scopelliti and K. Severin, *Inorg. Chem.*, 2012, **51**, 5795; (*j*) F. Linares, M. A. Galindo, S. Galli, M. A. Romero, J. A. R. Navarro and E. Barea, *Inorg. Chem.*, 2009, **48**, 7413.

7 (*a*) H. Takashima, S. Shinkai and I. Hamachi, *Chem. Commun.*, 1999, 2345; (*b*) J. Ohkanda, R. Satohb and N. Katoa, *Chem. Commun.*, 2009, 6949; (*c*) M. H. Filby, J. Muldoon, S. Dabb, N. C. Fletcher, A. E. Ashcroft and A. J. Wilson, *Chem. Commun.*, 2011, **47**, 559; (*d*) J. Muldoon, A. E. Ashcroft and A. J. Wilson, *Chem.–Eur. J.*, 2010, **16**, 100; (*e*) A. J. Wilson, J. R. Ault, M. H. Filby, H. I. A. Philips, A. E. Ashcroft and N. C. Fletcher, *Org. Biomol. Chem.*, 2013, **11**, 2206.

8 (*a*) S. Blanck, J. Maksimoska, J. Baumeister, K. Harms, R. Marmorstein and E. Meggers, *Angew. Chem., Int. Ed.*, 2012, **51**, 5244; (*b*) J. Maksimoska, L. Feng, K. Harms, C. Yi, J. Kissil, R. Marmorstein and E. Meggers, *J. Am. Chem. Soc.*, 2008, **130**, 15764; (*c*) E. Meggers, *Chem. Commun.*, 2009, 1001.

9 (*a*) M. J. Hannon, *Chem. Soc. Rev.*, 2007, **36**, 280; (*b*) G. I. Pascu, A. C. G. Hotze, C. S.-Cano, B. M. Kariuki and M. J. Hannon, *Angew. Chem., Int. Ed.*, 2007, **46**, 4374; (*c*) N. P. E. Barry, N. H. Abd Karim, R. Vilarand and B. Therrien, *Dalton Trans.*, 2009, 10717.

10 (*a*) A. Mishra, S. Ravikumar, S. H. Hong, H. Kim, V. Vajpayee, H. W. Lee, B. C. Ahn, M. Wang, P. J. Stang and K.-W. Chi, *Organometallics*, 2011, **30**, 6343; (*b*) A. Mishra, V. Vajpayee, H. Kim, M. H. Lee, H. Jung, M. Wang, P. J. Stang and K.-W. Chi, *Dalton Trans.*, 2012, **41**, 1195; (*c*) A. Mishra, H. Kim, S. C. Lee, J. W. Min, M. H. Lee and K.-W. Chi, *Inorg. Chim. Acta*, 2013, **405**, 77; (*d*) A. Mishra, H. Jung, M. H. Lee, M. S. Lah and K.-W. Chi, *Inorg. Chem.*, 2013, **52**, 8573.

11 (*a*) D. Groff, F. Wang, S. Jockusch, N. J. Turro and P. G. Schultz, *Angew. Chem., Int. Ed.*, 2010, **49**, 7677; (*b*) G. U. Nienhaus, *Angew. Chem., Int. Ed.*, 2008, **47**, 8992; (*c*) M. Swierczewska, G. Liu, S. Lee and X. Chen, *Chem. Soc. Rev.*, 2012, **41**, 2641.

12 (*a*) G. H. Patterson, S. M. Knobel, W. D. Sharif, S. R. Kain and D. W. Piston, *Biophys. J.*, 1997, **73**, 2782; (*b*) J. Zhang, R. E. Campbell, A. Y. Ting and R. Y. Tsien, *Nat. Rev. Mol. Cell Biol.*, 2002, **3**, 906.

13 J. K. Sanders and S. E. Jackson, *Chem. Soc. Rev.*, 2009, **38**, 2821.

14 H. Yan, G. Suss-Fink, A. Neels and H. Stoeckli-Evans, *J. Chem. Soc., Dalton Trans.*, 1997, 4345.

15 S. Shanmugaraju, A. K. Bar, S. A. Joshi, Y. P. Patil and P. S. Mukherjee, *Organometallics*, 2011, **30**, 1951.

16 D. B. Wetlaufer, *Adv. Protein Chem.*, 1962, **17**, 303.

17 R. Heim and R. Y. Tsien, *Curr. Biol.*, 1996, **6**, 178.

18 A. Kirchhofer, J. Helma, K. Schmidthals, C. Frauer, S. Cui, A. Karcher, M. Pellis, S. Muyldermans, C. S. Casas-Delucchi, M. C. Cardoso, H. Leonhardt, K. P. Hopfner and U. Rothbauer, *Nat. Struct. Mol. Biol.*, 2010, **17**, 133.

19 M. H. Kubala, O. Kovtun, K. Alexandrov and B. M. Collins, *Protein Sci.*, 2010, **19**, 2389.

20 A. T. Poulos, V. Kuzmin and N. E. Geacintov, *J. Biochem. Biophys. Methods*, 1982, **6**, 269.

21 S. McGinnis and T. L. Madden, *Nucleic Acids Res.*, 2004, **32**, W20.

22 *Protein Preparation Guide*, Schrodinger, LLC, 2010.

